Granular Matter
DOI 10.1007/s10035-013-0409-9

ORIGINAL PAPER

DEM investigation of particle anti-rotation effects on the micromechanical response of granular materials

Bo Zhou · Runqiu Huang · Huabin Wang · Jianfeng Wang

Received: 5 January 2013

Abstract The importance of particle rotation to the mechanical behavior of granular materials subject to quasi-static shearing has been well recognized in the literature. Although the physical source of the resistance to particle rotation is known to lie in the particle surface topography, it has been conveniently studied using the rolling resistance model installed typically on spherical particles within the DEM community. However, there has been little effort on assessing the capability of the rolling resistance model to produce more realistic particle rotation behavior as exhibited by irregular-shaped particles. This paper aims to eliminate this deficiency by making a comprehensive comparison study on the micromechanical behavior of assemblies of irregular-shaped particles and spherical particles installed with the rolling resistance model. A variety of DEM analysis techniques have been applied to elucidate the full picture of micromechanical processes occurring in the two types of granular materials with different particle-level anti-rotation mechanisms. Simulation results show that the conventional rheology-type rolling resistance models cannot reproduce the particle rotation and strain localization behavior as displayed by irregular-shaped materials, although they demonstrate clear effects on the macroscopic strength and dilatancy behavior, as have been adequately documented in the literature. More insights into the effects of particle-level anti-rotation mechanism are gained from an in-depth inter-particle energy dissipation analysis.

Keywords Anti-rotation · Energy input/output · Material localization · Anisotropy · DEM

B. Zhou · H. Wang
Department of Civil Engineering and Mechanics, Huazhong University of Science and Technology, Wuhan, China

B. Zhou · R. Huang
State Key Laboratory of Geohazard Prevention and Geo-environment Protection, Chengdu University of Technology, Chengdu, Sichuan Province, China

J. Wang (✉)
Department of Civil and Architectural Engineering, City University of Hong Kong, Kowloon, Hong Kong
e-mail: jefwang@cityu.edu.hk

1 Introduction

The particle-scale motion and interaction constitute the basis of the macroscopic mechanical properties of granular materials. Particle rotation, as an important microscopic deformation mechanism, is known to affect the macro-mechanical behavior of granular materials significantly and therefore has received extensive studies over the last two decades (e.g., [1–7]). For example, Iwashita and Oda [1] first pointed out that particle rotation highly affects the shear strength, dilation and material localization of granular materials by using the discrete element method (DEM). Kuhn and Bagi [2] and Alonso-Marroquin et al. [3] defined the interaction of a pair of particles as a combination of three modes: a contact deformation mode, a contact rolling mode, and a mode of rigid pair motion. The allocation of these three modes inside an assembly will control the displacement field, energy dissipation and bulk behavior of granular materials. Tordesillas and Walsh [5] incorporated rolling resistance and contact anisotropy into a micropolar constitutive model to simulate the behavior of granular materials. Recently, Zhang et al. [6] investigated the relationship between energy dissipation and shear band formation using DEM.

The physical source of the resistance to particle rotation lies in the particle surface topography. On a coarser scale, it has generally been referred to be the particle shape, which is

Published online: 23 March 2013

an essential geometrical factor controlling the fabric change of the granular materials under external loading conditions. Much experimental work has been done to investigate the particle shape effects on the behavior of sands. For example, the early tests conducted by Holubec and Appolonia [8] on medium fine sands with varying particle shapes indicated that granular materials with the same relative density could have different mechanical behavior due to different degrees of particle angularity. A series of triaxial tests on different types of sands [9,10] have shown that particle angularity and internal micro-fabric has a substantial effect on the shear strength, dilatancy and anisotropy behavior of sands. A common limitation of the conventional laboratory tests, however, is the little access to the micromechanics of a loaded sand.

As an alternative to the investigation of the fundamental soil behavior, the discrete element method first proposed by Cundall and Strack [11] has made significant contributions towards unraveling the micromechanical mechanisms of granular soil behavior over the past three decades [12–16]. On tackling the excessive and unrealistic amount of particle rotations that were frequently found in DEM simulations employing spherical particles and led to fictitious macroscopic material behavior, a number of authors (e.g., [1,17,18]) proposed to restrict the amount of particle rotation by employing the so-called "rolling resistance model" which was typically installed at existing particle contacts. The rolling resistance model often defines a rheology-type constitutive relationship between the contact couple and relative inter-particle rotation and operates in parallel with the conventional normal and tangential contact methods in DEM simulations. The first attempt to develop and implement such a model was perhaps made by Iwashita and Oda [1], who showed that the simulation data obtained using their modified discrete element method (MDEM) agreed better with experimental results. The MDEM was recently used by Mohamed and Gutierrez [4] in a comprehensive study on the effects of rolling resistance on elasticity, shear strength, dilation and bifurcation response of granular materials. Based on MDEM, Jiang et al. [18] proposed a physically and mathematically more rigorous rolling resistance model in which the general contact displacement was expressed in terms of pure rolling and pure sliding between two contacting discs. Comprehensive reviews of commonly used models of rolling resistance and discussions on different conditions for the application of various rolling resistance models can be found in Ai et al. [19] and Wensrich and Katterfeld [20].

As compared to the rolling resistance model, a more direct approach to get the more realistic particle rotation behavior is to incorporate irregular particle shapes into DEM simulations. This is typically achieved using the particle clump or cluster technique which creates irregular-shaped particles by bonding a group of elemental discs together. Using this technique, many authors (e.g., [21–26]) have studied the influence of various particle shape factors, such as roundness, angularity and elongation ratio etc. on the macroscopic mechanical response of granular materials. However, there has been little effort so far on assessing the capability of the rheology-type rolling resistance model to produce more realistic particle rotation behavior as exhibited by irregular-shaped particles [27]. More specifically, it is unclear whether the two kinds of particle-level anti-rotation mechanisms offered respectively by the rolling resistance model and the particle shape are equivalent in producing the macro- and micro-mechanical behavior of granular materials. To eliminate this deficiency, this paper aims to make a detailed comparison study on the macro- and micro-scopic behavior of granular assemblies composed of irregular-shaped particles and disc particles installed with the rolling resistance model. For the latter type of material, the Iwashita-Oda version of the rolling resistance model was employed for this study due to its simplicity and demonstrated performance of producing more realistic shear strength and dilatancy behavior. In-depth analyses of the DEM data were made to yield a comprehensive picture of the effects of the two kinds of particle anti-rotation mechanisms on the energy allocation, localization behavior of particle rotation, shear strain and inter-particle friction dissipation, as well as the shear-induced anisotropy of friction dissipation within the granular assemblies.

2 Methods

2.1 Modeling of particle shape

Many authors studied granular materials using ellipse-shaped or polygon-shaped particles in 2D and 3D DEM simulations (e.g., [28–31]). For example, Alonso-Marroquin and his co-workers [32–35] proposed an efficient method to generate complex-shaped particles based on Minkowski sum of sphere and polyhedron. However, a more popular and convenient technique to create irregular-shaped particles is the clump logic which employs a group of overlapping elemental discs to represent an ideal particle shape (e.g. ellipse or polygon) [24,25] or a random particle shape derived from digital image processing [36]. This technique was also used in this study to create two kinds of simple particle shapes: square and triangle. Specifically, a minimum number of elemental discs (i.e., 4 discs for square and 3 discs for triangle) was used and combined to approximate the intended particle shape. The size of a particle clump was given by the equivalent diameter (d) of another disc whose area is equal to the total area of the particle clump (i.e., counting the overlapping area only once). The clumped square and triangular particles and the equivalent disc are schematically shown in Fig. 1, with the relationships between the diameter of the composing disc of particle clump and its equivalent disc diameter shown in Table 1.

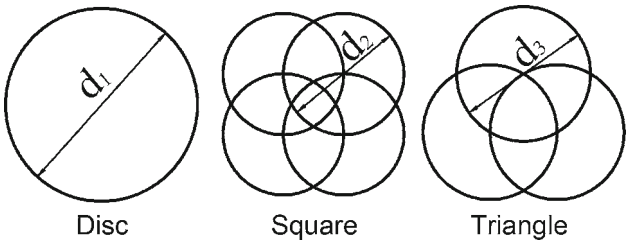

Fig. 1 *Square* and *triangular* particle clumps and their equivalent discs

Table 1 Diameter, shape factor and angularity factor of clumps and discs

Particle shape	Disc diameter	*SF*	*AF*
Disc	d_1	0	0
Square	$d_2 = d_1\sqrt{3\pi/(5\pi + 3\sqrt{3} + 3)}$	0.51	0.20
Triangle	$d_3 = d_1\sqrt{3\pi/(5\pi + 3\sqrt{3})}$	0.68	0.27

A variety of mathematical indexes have been proposed in the literature to characterize and quantify the particle shape factor (e.g., [37,38]). In this study, the normalized Shape Factor (*SF*) and Angularity Factor (*AF*) proposed by Sukumaran and Ashmawy [39] were adopted to characterize the shape effects of square and triangular particle clumps. The values of *SF* and *AF* for the two types of particle clumps and discs are also listed in Table 1. The higher values of both *SF* and *AF* of the triangular clump indicate its higher degree of shape irregularity and angularity. The readers are referred to Sukumaran and Ashmawy [39] for detailed definitions of *SF* and *AF*.

2.2 Modeling of rolling resistance for discs

The rolling resistance model proposed by Iwashita and Oda [1] was adopted in this study for the modeling of anti-rotation effects of discs. It is intended to compare the rolling resistance effects provided by this type of rheological particle contact model and those by particle shapes. The details of the rolling resistance model are briefly described below.

For a given assembly of interacting discs, consider one disc with a radius r surrounded with n contacts. At the $i\,th$ contact, the contact force F_i can be decomposed into a normal component N_i and a shear component T_i. Two types of kinematic inelastic behavior can occur for a contact: sliding and rolling. Sliding occurs when the shear component T_i exceeds the shear strength $T_{i\,\max}$ of the contact, which is defined as:

$$T_{i\,\max} = \mu \cdot |N_i|, \tag{1}$$

where μ is the friction coefficient of the contact.

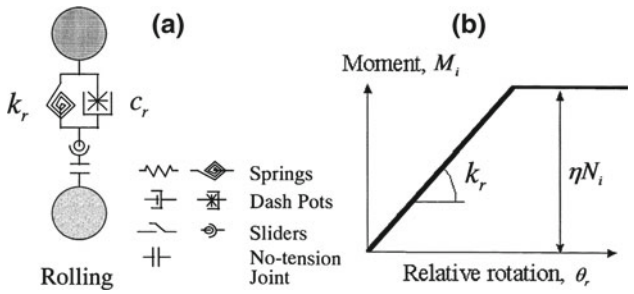

Fig. 2 **a** Contact model of rolling resistance; **b** constitutive relationship of the rolling resistance model (Ref. [1])

In the conventional DEM, rolling of a particle against another occurs without any resistance. The conservation law of angular momentum can be expressed as:

$$\sum_{i=1}^{n} T_i r = I\frac{d\omega}{dt}, \tag{2}$$

where I and ω are the moment of inertia and angular velocity of the particle respectively. However in reality, any particle contacts its neighboring particles at surfaces with finite areas and thus a moment of rolling resistance exists when a particle rolls over another. Denoting the moment of rolling resistance by M_i, Eq. (2) becomes:

$$\sum_{i=1}^{n} (T_i r + M_i) = I\frac{d\omega}{dt}, \tag{3}$$

The contact rolling model consists of an elastic spring, a dash pot, a no-tension joint and a slider, as shown in Fig. 2a. It provides two sources of rolling resistance:

$$M_i = -k_r\theta_r - C_r\frac{d\theta_r}{dt}, \tag{4}$$

where k_r is the rolling stiffness, C_r is the viscosity coefficient, and θ_r is the relative rotation between two particles. C_r is set to zero in the present study as the second term of Eq. (4) only serves to stabilize the numerical computation and has little effect on the quasi-static simulation results. Bardet and Huang [40] derived the analytical expression of k_r as:

$$k_r = -2r N_i J_n, \tag{5}$$

where J_n varies from 0.25 to 0.5. Since perfectly rigid discs are used in the current study, J_n takes the value of 0.5 in all the simulations.

It is assumed that perfectly plastic rolling will occur if M_i exceeds a threshold value ηN_i, meaning that a particle will start to roll without mobilizing any further rolling resistance above the threshold value (Fig. 2b).

$$M_i \le \eta N_i, \tag{6}$$

The parameter η was first defined by Sakaguchi et al. [41] as the coefficient of rolling resistance, which has a dimension of length based on Eq. (6). In the present study, η takes the

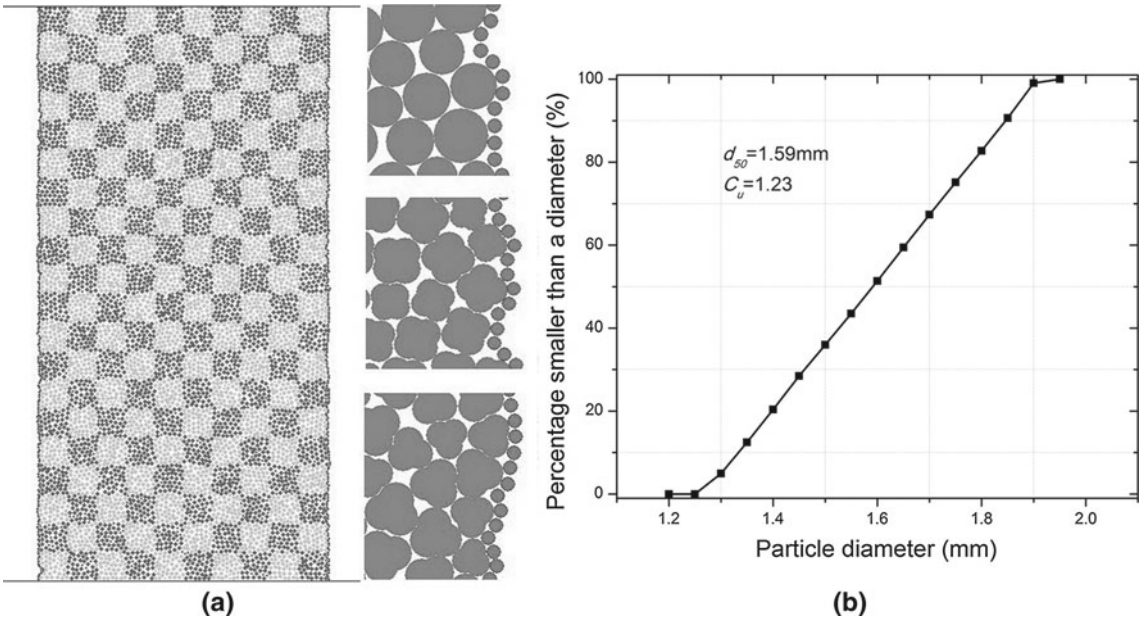

Fig. 3 **a** DEM sample with flexible membrane boundaries; **b** particle size distribution of the samples

values of 10^{-7}, 10^{-5} and 10^{-3} m representing three drastically different levels of rolling resistance. It is intended to make a detailed comparison study on the micromechanical behavior of granular samples under the influence of varying η values and particle shape factors (i.e., *SF* & *AF*).

3 DEM sample preparation and testing

All the DEM simulations were conducted using PFC^{2D} [42] in this study. Each sample has a dimension of 100 mm (W) × 200 mm (H) and contains 8,355 particles (Fig. 3a). The particle size distribution is shown in Fig. 3b. The samples have a mean particle diameter (d_{50}) of 1.59 mm and a uniformity coefficient C_u ($C_u = d_{60}/d_{10}$) of 1.23. For irregular particles, the particle size is referred to be the equivalent diameter of the particle clump. All the samples are first generated using disc particles within a rectangular container with all wall boundaries and the location of each disc is recorded. For irregular-shaped samples, each disc in the assembly is replaced by a particle clump whose size and center coincide with those of the disc. After all the samples are generated, the two side walls are replaced by two flexible membrane boundaries [43–45]. Composing of a single layer of contact-bonded discs which each can freely move and rotate, the membrane boundaries are capable of maintaining better the uniform distribution of the confining pressure during the shearing process [46,47]. All the samples are then consolidated under the isotropic confining pressure of 100 kPa to reach the initial equilibrium condition. The sample porosity after consolidation is about 0.16 and is attained by using a low inter-particle friction coefficient of 0.1.

During the subsequent shearing process, the top and the bottom walls move forwards each other at a constant strain rate of 6 % per minute while the side membrane boundaries maintain the constant confining pressure of 100 kPa. The DEM parameters of discs, particle clumps and membrane particles are summarized in Table 2. It needs to be mentioned that a local, non-viscous damping model which is appropriate for the quasi-static simulations and available in PFC^{2D} was adopted in this study. In this damping model, the damping force acting on each particle is proportional to the total unbalanced force through the damping coefficient α. Detailed discussions on the effects of α on the particle-scale energy dissipation behavior of ideal assemblies of rigid discs with rolling resistance and crushable particle clusters can be found in Zhang et al. [6] and Wang and Yan [47], respectively.

In the following sections, we report detailed simulation results from five simulations, with the first three on disc samples with varying η values and the other two on square and triangle clump samples. In-depth micromechanical analyses on the particle-scale energy storage/dissipation, accumulated particle rotation, strain localization and shear banding, as well as shear-induced anisotropies of inter-particle friction dissipation are presented.

4 Results and discussions

4.1 Macroscopic mechanical behavior

Figure 4 shows the deviatoric stress ratio t/s ($t = (\sigma_1 - \sigma_3)/2$, $s = (\sigma_1 + \sigma_3)/2$) and volumetric strain versus axial

Table 2 DEM parameters of discs, clump particles and membrane discs

Discs/clumps	Density (kg m^{-3})	2,600
	Diameter range (mm)	1.24–1.96
	Contact normal stiffness (N m^{-1})	8×10^7
	Contact shear stiffness (N m^{-1})	8×10^7
	Porosity	0.16
	Inter-particle friction coefficient	0.5
	Inter-particle rolling resistance coefficient (m)	10^{-7}, 10^{-5}, 10^{-3}
	Local damping coefficient	0.5
Membrane discs	Diameter (mm)	0.5
	Normal bond strength (N)	1×10^{50}
	Shear bond strength (N)	1×10^{50}
	Contact normal stiffness (N m^{-1})	8×10^6
	Contact shear stiffness (N m^{-1})	8×10^6
	Friction coefficient	0.0

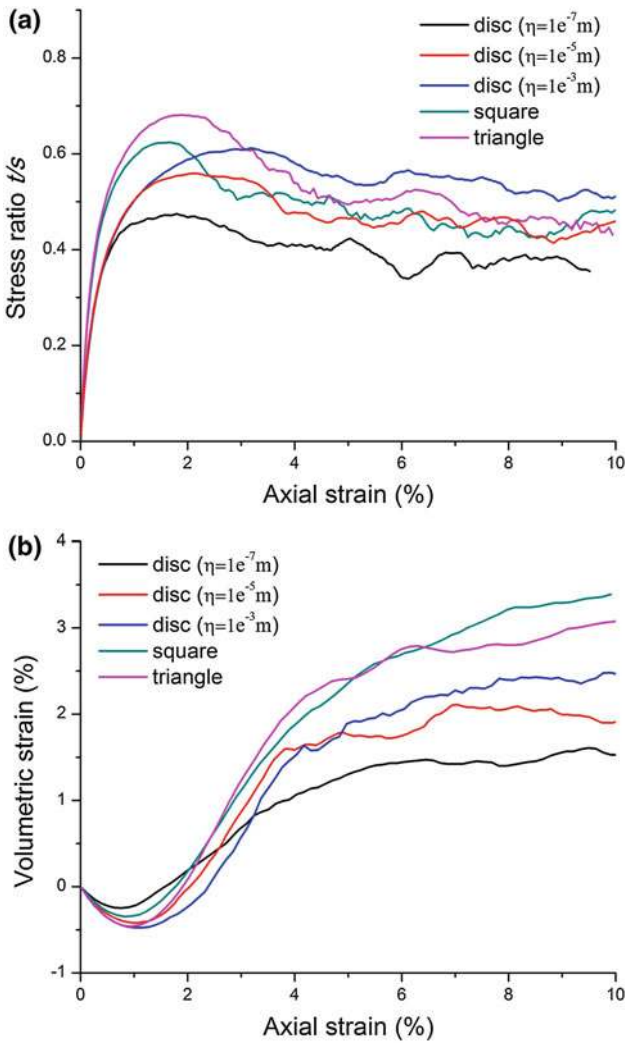

Fig. 4 Macroscopic behavior of DEM simulations: **a** deviatoric stress ratio versus axial strain; **b** volumetric strain versus axial strain

strain relationships from all the five simulations. It is clear that the two particle clump samples with high *SF/AF* value exhibit overall higher peak stress ratios than the disc samples, although raising the η value results in an obvious increase of the peak stress ratio of the disc samples (Fig. 4a). Correspondingly, increasing dilatancy of the disc samples with the increasing η value is also observed but remains distinctly lower than that of the clump samples (Fig. 4b). It is possible to attain a peak stress ratio similar to that of the square clump sample by setting an artificial high η value of 10^{-3} m. Moreover, the applied axial strain at which the peak stress ratio is reached also increases with the increasing η value for disc samples, and is overall much greater than those of the clump samples. Apparently, the higher macroscopic shear strength of the disc sample with the higher η value is attributed to the enhanced capacity of the assembly to absorb more strain energy with the help of a greater degree of the particle rotation. More microscopic evidences will be presented below to support this statement. However, it seems impossible to achieve the level of the peak stress ratio exhibited by a highly irregular clump sample like the triangle clump sample by just adjusting the η value for the disc sample. This observation indicates that the high geometric effects of particle interlocking cannot be simply reproduced by setting an artificial high rolling resistance effect for disc particles.

4.2 Particle-scale energy input and dissipation

It is widely accepted that the energy behavior is of critical importance to establishing the linkage between micro- and macro-mechanical responses. For granular materials, the particle-level energy input/output behavior can be readily studied using the discrete element method [47,48]. Next, we examine the evolutions of energy input and dissipation by tracing the various energy components in the incremental

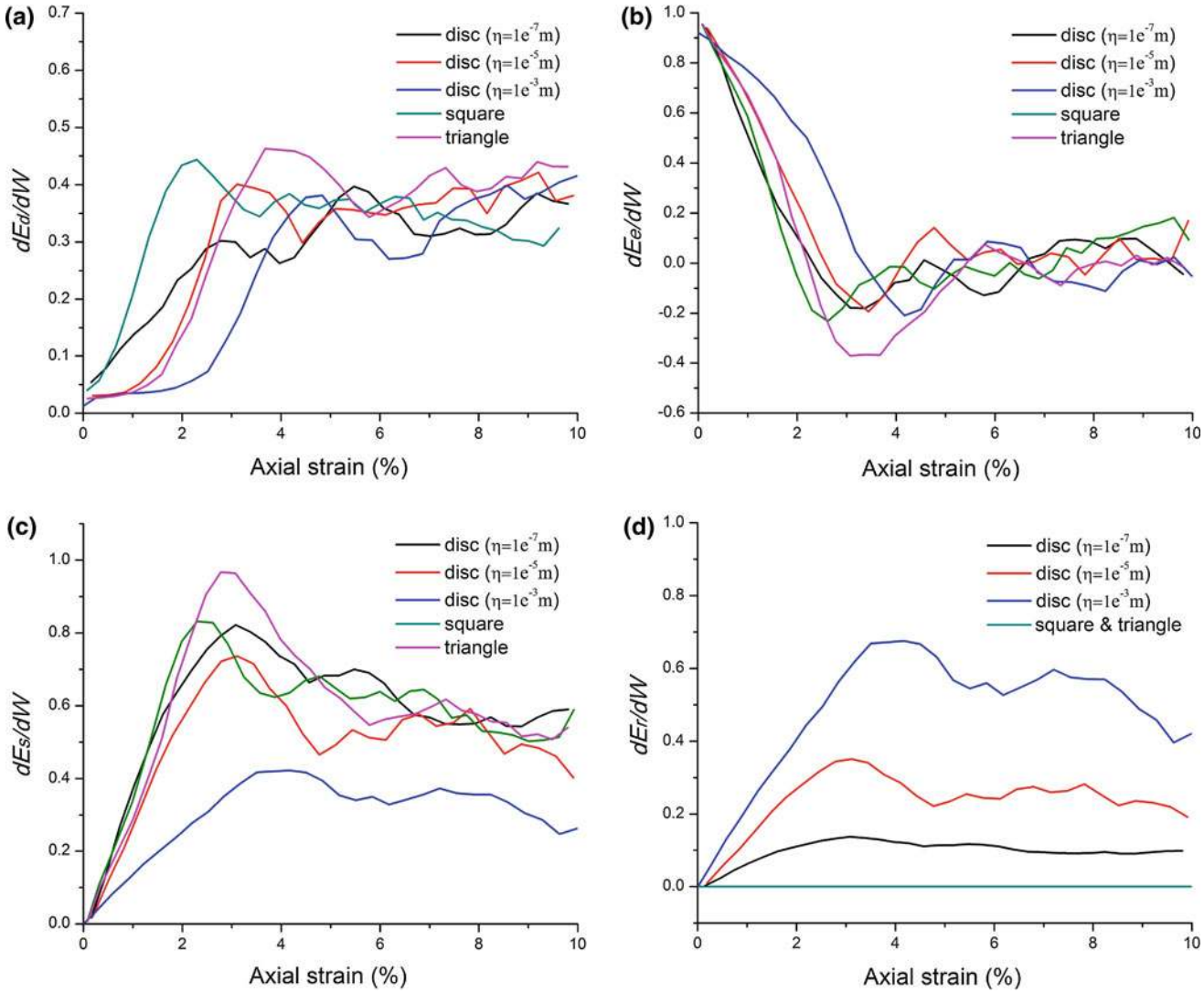

Fig. 5 Evolutions of various incremental energy ratios against the axial strain

form during the shearing process. It is convenient to trace the following types of energy terms in the DEM simulations: input boundary work dW, body work dW_g, elastic strain energy dE_e stored at particle contacts, inter-particle friction dissipation dE_f, kinetic energy dE_k, and damping dissipation dE_d. In this study, the body work dW_g is equal to zero because the soil gravity acceleration was set to zero. For unbonded particles, the contact bond energy is also not considered. For disc particles with rolling resistance, the inter-particle friction dissipation dE_f is composed of two parts: sliding dissipation dE_s and rolling dissipation dE_r [6]. They were calculated by summing the slip work and the rolling work, respectively, as follows:

$$dE_s = \sum_{N_s} \left[\langle T_i \rangle \cdot (dU_i)^{slip} \right], \tag{7}$$

$$dE_r = \sum_{N_r} \left[\langle M_i \rangle \cdot (d\theta_i)^{roll} \right], \tag{8}$$

where N_s and N_r are the total number of sliding and rolling contacts, respectively; $\langle T_i \rangle$ and $\langle M_i \rangle$ are the average values of shear forces and moments at the start and end of the current step; and $(dU_i)^{slip}$ and $(d\theta_i)^{roll}$ are the increments of sliding displacement and relative rotation, respectively. Due to the quasi-static nature of the simulations, the kinetic energy dE_k will be negligible in comparison to dE_e, dE_s, dE_r and dE_d.

Figure 5 shows the evolution of various incremental energy ratios against the axial strain from all the simulations. The incremental energy ratios, which are defined as the incremental energy storage/dissipation terms normalized with respect to the incremental boundary work, i.e., dE_e/dW, dE_s/dW, dE_r/dW and dE_d/dW, essentially

reflect the way in which the external work is allocated at the microscopic level. The same incremental axial strain of 0.3 % was used in all the simulations to compute the incremental energy ratios shown in Fig. 5.

Based on the energy conservation principle and neglecting the kinetic energy dE_k, the sum of the four energy ratio terms shown in Fig. 5 is approximately equal to 1.0 at any instance during the shearing process. It is seen that the most severe change of the energy allocation mode occurs within the first 5 % strain, where significant variations of the four energy ratio terms are observed. At large strains, all the energy ratios become nearly constant, implying a relatively steady energy allocation mode featuring the critical state of the granular sample. Apparently, for disc samples, increasing the η value 10^4 times has resulted in: (1) a lateral shift of the dE_d/dW curve implying similar steady-state magnitudes reached at an increasing strain level (Fig. 5a); (2) the distinct decrease of the initial slope of the dE_e/dW curve (Fig. 5b); (3) the significant decreases of the initial slope and peak and steady state magnitudes of the dE_s/dW curve (Fig. 5c); (4) the significant increases of the initial slope and peak and steady state magnitudes of the dE_r/dW curve (Fig. 5d). A more comprehensive discussion on the rolling resistance effects on the energy allocation mode in a disc sample has been made in Zhang et al. [6].

However, the salient features of the energy ratio curves of the two clump samples as compared to those of the disc samples and their implications on the macroscopic shear strength behavior need to be highlighted. Since no rolling resistance model was used for particle clumps, dE_r/dW is always equal to zero in clump samples. As a result, there is not much difference between the profiles of dE_s/dW and dE_e/dW of the two clump samples and those of the disc sample with $\eta = 10^{-7}$ m which only offers a low amount of rolling resistance, especially within the small-strain range up to the peak point. However, the much higher peak stress ratios of the clump samples are consistent with their initial lower slopes of the dE_e/dW curves before the peak point, which suggests the slower rate of the decay of the capability of the sample to store elastic strain energy due to the high particle interlocking effects. The significant gain of the peak stress ratio of the disc sample due to the increase of η value is also reflected in the marked reduction of the initial slope of the dE_e/dW (getting even lower than that of the triangular clump sample). It should be noted, however, that the now enhanced capacity of the sample to store elastic strain energy stems from the significant amount of particle rotation allowed by the high rolling resistance. Because of this, it takes a much larger strain to fully mobilize the shear strength than clump samples which rely on particle interlocking to develop the shear strength. A natural consequence of the enhanced particle rotation is the prevalence of inter-particle rolling dissipation against inter-particle sliding dissipation.

4.3 Localizations of particle rotation, shear strain and friction dissipation

To better understand the micromechanical origin of the anti-rotation effects on the macroscopic shear strength behavior, we further examine the localization phenomena of particle rotation, shear strain and inter-particle friction dissipation. Figures 6 and 7 show the spatial distributions of the accumulated quantities of the three variables from all the simulations at the peak state and the critical state (10 % axial strain), respectively. The accumulated rotation of a particle clump can be readily obtained since it is exactly the same as that of any composing disc given that no internal deformation is allowed among all the composing discs forming a rigid body of the clump. The accumulated shear strain here refers to the local material shear deformation as opposed to the bulk shear deformation measured from the sample boundary. The shear strain distribution was calculated using the mesh-free strain calculation method developed by Wang et al. [49]. This method can accurately account for the material shear deformation caused by particle rotation [6,15,50,51]. The spatial distributions of the accumulated inter-particle friction dissipations, which includes the sliding and rolling dissipations for disc samples, were obtained by recording in every time step all the sliding and rolling work and their locations of occurrence which are taken to be the current positions of the corresponding contacts. A total number of 31,250 pixels with a pixel size of 0.8 mm $\times$ 0.8 mm was used in the construction of the final plots, implying that the value of each pixel was equal to the sum of all the friction work taking place in that particular pixel subdomain.

It is found in Figs. 6 and 7 that generally very good agreement exists among the localization patterns of the three variables at the peak and the critical states, indicating their consistency in depicting the localization mechanism of the granular materials. Distinct localization bands of the three variables are observed in all the five simulations at the critical state (Fig. 7). However at the peak state, the localization patterns of different samples exhibit more disparities. It is clear that the disc samples already developed an incipient configuration of the major shear band at the peak state which was recognized to be consistent with the ultimate shear band at the critical state, and such a trend seems to become more pronounced with the increasing η values; nevertheless, for the two clump samples with high *SF/AF* values, highly dispersive patterns of localization are given by the particle rotation and shear strain at the peak state, giving no clue of the ultimate major shear bands found at the critical state. This interesting observation suggests that the high macroscopic shear strength of a clump sample is indeed caused by a globally more 'uniform' localization of the microscopic particle movement (i.e. sliding and rotation). Therefore, the rolling resistance model of disc samples and the particle interlocking

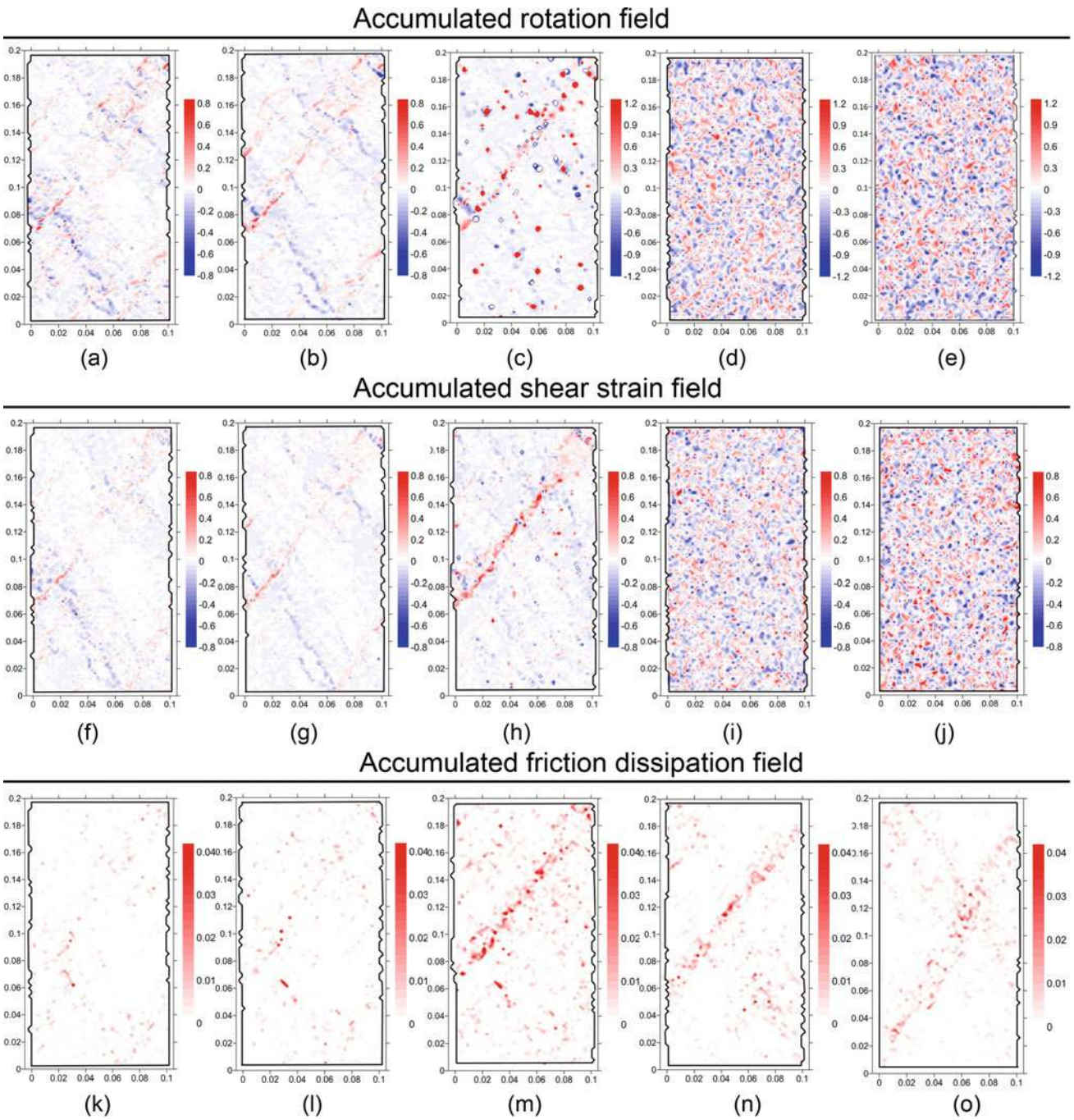

Fig. 6 Spatical distributions of accumulated particle rotation, shear strain and inter-particle friction dissipation at the peak state

effects of clump samples produce drastically different material localization behaviors that underlie the macroscopic shear strength behavior. More insights of the above observation can be obtained from the probability distributions of the sliding friction mobilization index I_m from all the simulations at the peak state, as shown in Fig. 8.

The sliding friction mobilization index I_m of a particle contact is defined as [52]

$$I_m = \frac{|T_i|}{\mu N_i}, \tag{9}$$

Interestingly, the distribution profiles of the disc samples show marked differences from those of the clump samples: the former being biased towards both low (i.e., $I_m = 0.1$) and high (i.e., $I_m = 1.0$) ends of the I_m range, with a nearly linear reduction of the probability from $I_m = 0.1$ to $I_m = 0.7$;

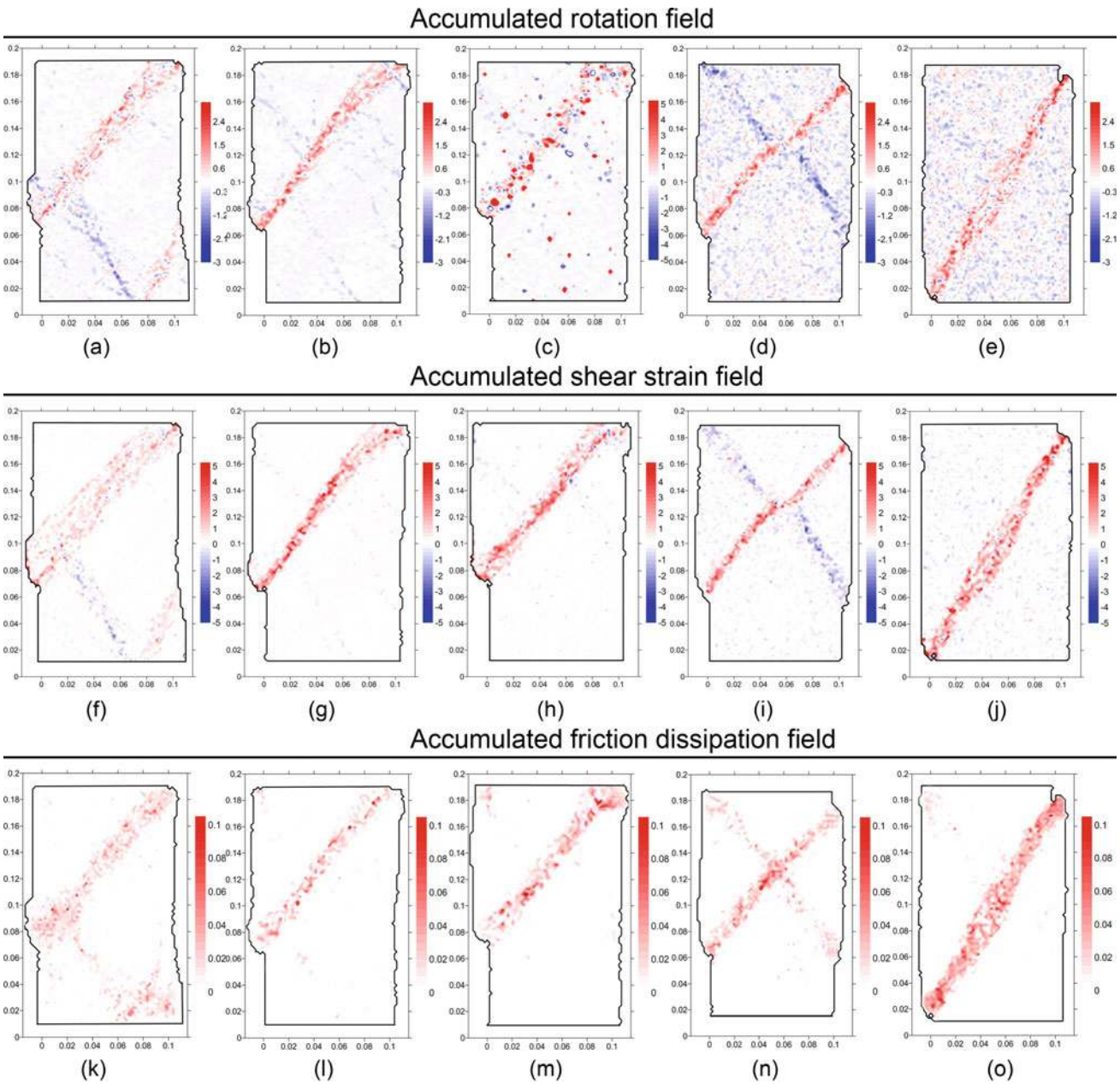

Fig. 7 Spatical distributions of accumulated particle rotation, shear strain and inter-particle friction dissipation at the critcal state (i.e., 10 % strain)

while the latter being only biased towards the high end (i.e., $I_m = 1.0$) of the I_m range, with a nearly constant probability between $I_m = 0.1$ to $I_m = 0.8$. This result suggests a more uniform gradient of the sliding friction mobilization from the center of the incipient shear band towards the less localized parts in disc samples. More importantly, the probability values of the two clump samples at $I_m = 1.0$ are much higher than those of the disc samples, indicating that the numbers of particle contacts that are experiencing sliding at the peak state are much greater in the clump samples. This is again the result caused by the high particle interlocking. Additionally, the in-set diagram of Fig. 8 indicates that the average I_m value is linearly correlated with the particle anti-rotation level, with the triangular clump sample having the highest I_m value of 0.59.

It is also interesting to note that the localization bands of inter-particle friction dissipation appear more distinctive at both peak and critical states, largely lacking of the background noises seen in those of the particle rotation and shear strain. This observation indicates that the localization of plas-

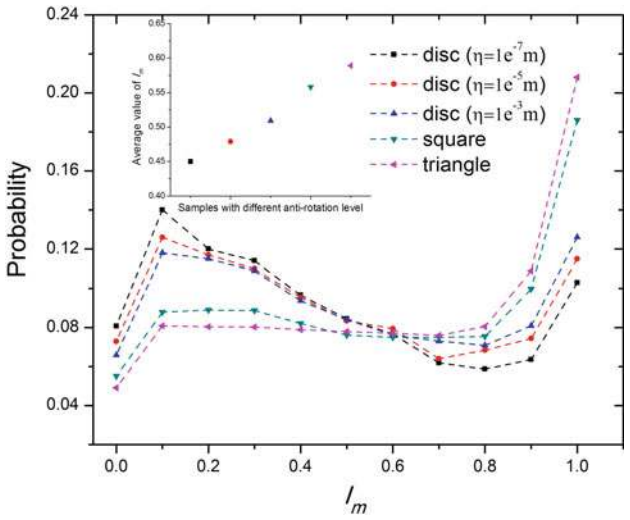

Fig. 8 Probability distribution of friction mobilization index I_m at the peak state

tic dissipation realized by inter-particle rolling and sliding in a more essential representation of the shear-induced instability mechanism of granular materials.

4.4 Anisotropy of accumulated inter-particle friction dissipation

Given the high fundamental importance of the inter-particle friction dissipation, it is finally essential to examine its polar distributions during the shearing process. Figure 9 shows such plots at the peak and the critical states from all the simulations. The construction of a polar distribution differs from that of a spatial distribution in that the spatial coordinate of any particular incremental friction dissipation work is replaced by its orientational coordinate, which is taken to be the tangential direction of the corresponding contact. In the construction of the final plots, a total number of 36 fractions with each fraction covering a 10° interval were used, and the sum of the accumulated friction dissipation in each fraction is normalized by the average friction dissipation over all the fractions to obtain the normalized dissipation.

It is seen in Fig. 9 that each plot of polar distribution exhibits marked anisotropy characteristics, but the degree of anisotropy decreases slightly with the increasing axial strain level, especially for the clump samples and the disc sample with the low η value (i.e., $\eta = 10^{-7}$ m). More importantly, all the polar distribution plots show two distinct principal directions of the accumulated friction dissipation, which is in contrast to the single localization band of friction dissipation found in Figs. 6k–o and 7k–o. This interesting phenomenon suggests that nearly equal amounts of the accumulated friction dissipation take place in two roughly orthogonal principal directions although the majority of them are physically located within one single dissipation band. Such a result is attributed to the complicated coupling effects of inter-particle sliding and rolling within the friction dissipation band. When a higher amount of particle rotation is allowed, like in the

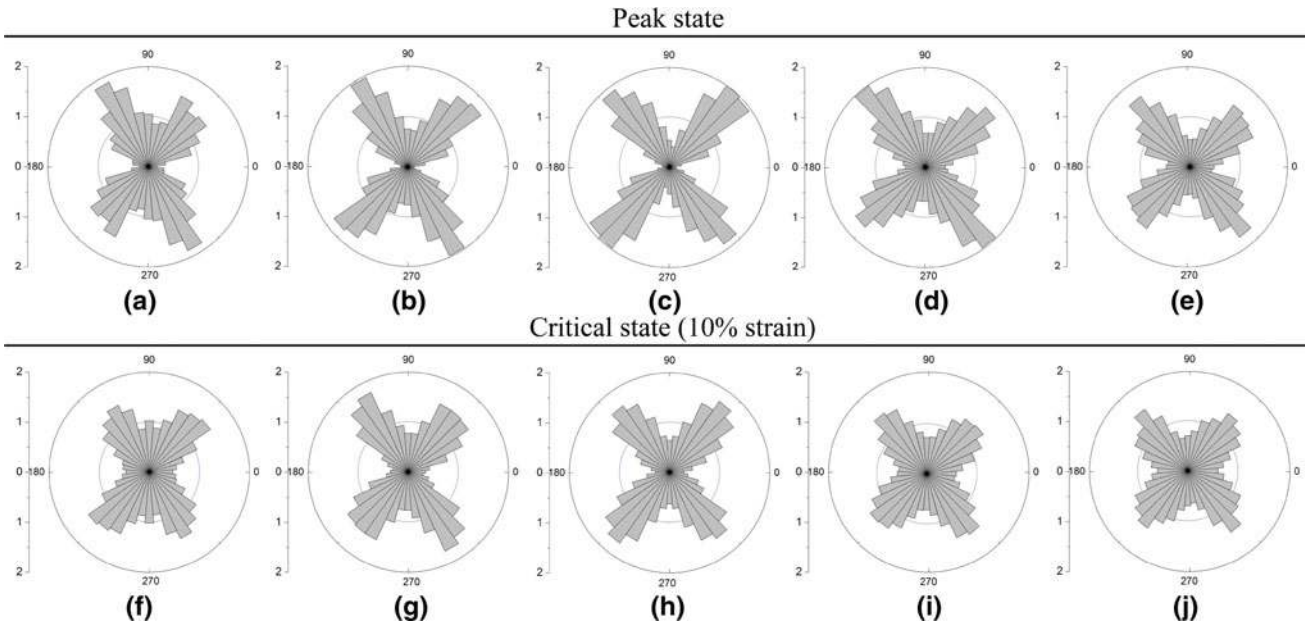

Fig. 9 Normalized polar distributions of accumulated inter-particle friction dissipation. **a–e** at peak state; **f–j** at critical state (i.e., 10 % strain)

cases of the two clump samples and the disc sample with $\eta = 10^{-7}$m (Fig. 9f, i, j), the degree of the anisotropy of the polar distribution tends to reduce because the direction of any inter-particle sliding/rolling dissipation tends to be more random.

5 Conclusion

This paper reports the results from a 2D DEM study on the effects of two different kinds of particle-level anti-rotation mechanisms, namely, the rheology-type rolling resistance model and the irregular particle shape, on the macro- and micro-scopic mechanical response of granular materials. A variety of DEM analysis techniques were applied to achieve a comprehensive understanding of the micromechanics occurring within the two types of granular materials.

Simulation data show that both mechanisms of particle anti-rotation result in enhanced shear strength and dilatancy behavior of granular assemblies, which are attributed to the enhanced capacity of the granular assemblies to store elastic strain energy. However, this macroscopic result is achieved through a higher amount of particle rotation in a disc sample but through a higher particle interlocking effect in an irregular-shaped clump sample. The different particle anti-rotation mechanisms create some essential difference in the localization modes of particle rotation and shear strain at the peak state between the two types of materials, with the disc samples exhibiting a clear localization band while the clump samples exhibiting a more 'uniform' localization pattern. This finding leads to the major conclusion of this paper that the rheology-type rolling resistance model cannot replace the particle shape effects for a simulation purpose to achieve the more realistic and physically sound constitutive behavior of granular materials due to their fundamental disparity in the material localization behavior. However, it is also interesting to note that the difference between the two types of materials diminishes when the localization of the inter-particle friction dissipation is concerned. Moreover, due to complicated coupling effects of inter-particle sliding and rolling within the friction dissipation band, nearly equal amounts of the accumulated friction dissipation take place in two roughly orthogonal principal directions although most of them are physically located within one single dissipation band.

Acknowledgments This research was financially supported by National Science Foundation of China for Young Investigators with Grant No. 51109182, Research Grant No. SKLGP2012K019 from the State Key Laboratory of Geohazard Prevention and Geo-environment Protection of Chengdu University of Technology, Strategic Research Grant No. 7008180 from City University of Hong Kong, Grant No. 2012BAK10B00 from Ministry of National Science and Technology and Key Program No. 2009CDA007 of Natural Science Foundation of Hubei.

References

1. Iwashita, K., Oda, M.: Rolling resistance at contacts in simulation of shear band development by DEM. J. Eng. Mech. ASCE **124**, 285–292 (1998)
2. Kuhn, M.R., Katalin, B.: Contact rolling and deformation in granular media. Int. J. Solids Struct. **41**(21), 5793–5820 (2004)
3. Alonso-Marroquin, F., Vardoulakis, I., Herrmann, H.J., Weatherley, D., Mora, P.: Effect of rolling on dissipation in fault gouges. Phys. Rev. E **74**(3), 031306 (2006)
4. Mohamed, A., Gutierrez, M.: Comprehensive study of the effects of rolling resistance on the stress–strain and strain localization behavior of granular materials. Granul. Matter **12**, 527–541 (2010)
5. Tordesillas, A., Walsh, D.C.: Incorporating rolling resistance and contact anisotropy in micromechanical models of granular media. Powder Technol. **124**(1), 106–111 (2002)
6. Zhang, W.C., Wang, J.F., Jiang, M.J.: DEM-aided discovery of the relationship between energy dissipation and shear band formation considering the effects of particle rolling resistance. J. Geotech. Geoenviron. Eng., online first (2013). doi:10.1061/(ASCE)GT.1943-5606.0000890
7. Astrom, J.A., Timonen, J.: Spontaneous formation of densely packed shear bands of rotating fragments. Eur. Phys. J. E **35**(40), 1–5 (2012)
8. Holubec, I., D'Appolonia, E.: Effect of particle shape on the engineering properties of granular soils. Am. Soc. Test. Mater. ASTM STP **523**, 304–318 (1973)
9. Guo, P., Su, X.: Shear strength, interparticle locking, and dilatancy of granuar materials. Can. Geotech. J **44**(5), 579–591 (2007)
10. Tsomokos, A., Georgiannou, V.N.: Effect of grain shape and angularity on the undrained response of fine sands. Can. Geotech. J. **47**(5), 539–551 (2010)
11. Cundall, P.A., Strack, O.D.: A discrete numerical-model for granular assemblies. Geotechnique **29**, 47–65 (1979)
12. Emeriault, F., Chang, C.S.: Interparticle forces and displacements in granular materials. Comput. Geotech. **20**(3–4), 223–244 (1997)
13. Sitharam, T.G.: Micromechanical modeling of granular materials: effect of confining pressure on mechanical behavior. Mech. Mater. **31**(10), 653–665 (1999)
14. Liu, S.H., Matsuoka, H.: Microscopic interpretation on a stress–dilatancy relationship of granular materials. Soils Found. **43**(3), 73–84 (2003)
15. Wang, J., Gutierrez, M.S.: Discrete element simulations of direct shear specimen scale effects. Géotechnique **60**(5), 395–409 (2010)
16. Guo, P.: Critical length of force chains and shear band thickness in dense granular materials. Acta Geotech. **7**, 41–55 (2012)
17. Iwashita, K., Oda, M.: Micro-deformation mechanism of shear banding process based on modified distinct element method. Powder Technol **109**, 192–205 (2000)
18. Jiang, M.J., Yu, H.S., Harris, D.: A novel discrete model for granular material incorporating rolling resistance. Comput. Geotech. **32**, 340–357 (2005)
19. Ai, J., Chen, J., Rotter, J.M., Ooi, J.Y.: Assessment of rolling resistance models in discrete element simulations. Powder Technol. **206**, 269–282 (2011)
20. Wensrich, C.M., Katterfeld, A.: Rolling friction as a technique for modelling particle shape in DEM. Powder Technol. **217**, 409–417 (2012)
21. Nouguier-Lehon, C., Cambou, B., Vincens, E.: Influence of particle shape and angularity on the behaviour of granular materials:

a numerical analysis. Int. J. Numer. Anal. Methods Geomech. **27**, 1207–1226 (2003)
22. Nouguier-Lehon, C.: Effect of the grain elongation on the behaviour of granular materials in biaxial compression. Computes Rendus Mecanique **338**, 587–595 (2010)
23. Antonya, S.J., Momoha, R.O., Kuhnb, M.R.: Micromechanical modelling of oval particulates subjected to bi-axial compression. Comput. Mater. Sci. **29**, 494–498 (2004)
24. Mahmood, Z., Iwashita, K.: Influence of inherent anisotropy on mechanical behavior of granular materials based on DEM simulations. Int. J. Numer. Anal. Methods Geomech. **34**, 795–819 (2010)
25. Mahmood, Z., Iwashita, K.: A simulation study of microstructure evolution inside the shear band in biaxial compression test. Int. J. Numer. Anal. Methods Geomech. **35**, 652–667 (2011)
26. Abedi, S., Mirghasemi, A.A.: Particle shape consideration in numerical simulation of assemblies of irregularly shaped particles. Particulology **9**, 387–397 (2011)
27. Estrada, N., Azema, E., Radjai, F.: Identification of rolling resistance as a shape parameter in sheared granular media. Phys. Rev. E **84**(1), 011306 (2011)
28. Favier, J.F., et al.: Shape representation of axisymmetrical, nonspherical particles in discrete element simulation using multi-element model particles. Eng. Comput. **16**(4), 467–480 (1999)
29. Matuttis, H.G., Luding, S., Herrmann, H.J.: Discrete element simulations of dense packings and heaps made of spherical and nonspherical particles. Powder Technol. **109**, 278–292 (2000)
30. Bagherzadeh-Khalkhali, A., Mirghasemi, A.A., Mohammadi, S.: Micromechanics of breakage in sharp-edge particles using combined DEM and FEM. Particuolagy **6**, 347–361 (2008)
31. Bagherzadeh-Khalkhali, A., Mirghasemi, A.A.: Numerical and experimental direct shear tests for coarse-grained soils. Particuolagy **7**, 83–91 (2009)
32. Alonso-Marroquin, F., Luding, S., Herrmann, H.J., Vardoulakis, I.: Role of anisotropy in the elastoplastic response of a polygonal packing. Phys. Rev. E **71**, 051304 (2005)
33. Alonso-Marroquin, F.: Spheropolygons: a new method to simulate conservative and dissipative interactions between 2D complex-shaped rigid bodies. Europhys. Lett. **83**, 14001 (2008)
34. Alonso-Marroquín, F., Wang, Y.: An efficient algorithm for granular dynamics simulations with complex-shaped objects. Granul. Matter **11**, 317–329 (2009)
35. Galindo-Torres, S.A., Munoz, J.D., Alonso-Marroquin, F.: Minkowski-Voronoi diagrams as a method to generate random packings of spheropolygons for the simulation of soils. Phys. Rev. E **82**, 056713 (2010)
36. Ashmawy, A.K., Sukumaran, B., Hoang, V.V.: Evaluating the influence of particle shape on liquefaction behavior using discrete element modeling. In: Proceedings of The 13th (2003) International Offshore And Polar Enginerring Conference, vol. 2, pp. 542–549 (2003)
37. Riley, N.A.: Projection sphericity. J. Sediment. Petrol **11**, 94–97 (1941)
38. Blott, S.J., Pye, K.: Particle shape: a review and new methods of characterization and classification. Sedimentology **55**(1), 31–63 (2008)
39. Sukumaran, B., Ashmawy, A.K.: Quantitative characterisation of the geometry of discrete particles. Geotechnique **51**(7), 619–627 (2001)
40. Bardet, J.P., Huang, Q.: Rotational stiffness of cylindrical particle contacts. In: Proceeding on 2nd International Conference on Micromechanics of Granular, Media, pp. 39–43 (1993)
41. Sakaguchi, H., Ozaki, E., Igarashi, T.: Plugging of the flow of granular materials during the discharge from a silo. Int. J. Mod. Phys. B **7**, 1949–1963 (1993)
42. Itasca: PFC2D Manual (Version 4.0). Itasca Consulting Group Inc, Minneapolis (2008)
43. Astrom, J.A., Herrmann, H.J., Timonen, J.: Granular packings and fault zones. Phys. Rev. Lett. **84**(4), 638–641 (2000)
44. Alonso-Marroquin, F., Herrmann, H.J.: Calculation of the incremental stress–strain relation of a polygonal packing. Phys. Rev. E **66**(2), 021301 (2002)
45. Wang, Y.H., Leung, S.C.: Characterization of cemented sand by experimental and numerical investigations. J. Geotech. Geoenviron. Eng. ASCE **134**(7), 992–1004 (2008)
46. Wang, J., Yan, H.B.: On the role of particle breakage in the shear failure behavior of granular soils by DEM. Int. J. Numer. Anal. Methods Geomech, Online first (2011). doi:10.1002/nag
47. Wang, J., Yan, H.B.: DEM analysis of energy dissipation in crushable soils. Soils Found. **52**(4), 644–657 (2012)
48. Bolton, M.D., Nakata, Y., Cheng, Y.P.: Micro-and macro-mechanical behavior of DEM crushable materials. Geotechnique **58**(6), 471–480 (2008)
49. Wang, J., Gutierrez, M.S., Dove, J.E.: Numerical studies of shear banding in interface shear tests using a new strain calculation method. Int. J. Numer. Anal. Meth. Geomech. **31**(12), 1349–1366 (2007a)
50. Wang, J., Dove, J.E., Gutierrez, M.S.: Discrete-continuum analysis of shear band in the direct shear test. Géotechnique **57**(6), 527–536 (2007b)
51. Wang, J., Jiang, M.J.: Unified soil behavior of interface shear test and direct shear test under the influence of lower moving boundaries. Granul. Matter **13**(5), 631–641 (2011)
52. Azema, A., Radja, F.: Force chains and contact network topology in sheared packings of elongated particles. Phys. Rev. E **85**, 031303 (2012)